# Effect of CaO Addition on Nickel Catalysts Supported on Alumina for Glycerol Steam Reforming

João Paulo da S. Q. Menezes[1] · Flávia C. Jácome[1] · Robinson L. Manfro[1] · Mariana M. V. M. Souza[1]

## Abstract

Hydrogen production by glycerol steam reforming is an attractive alternative, as it represents the conversion of a waste in a high-added value product. In this work, three catalysts were synthesized by wet impregnation of nickel precursor in different supports: $\gamma$-Al$_2$O$_3$ prepared by boehmite calcination, $\alpha$-Al$_2$O$_3$ and 15 wt% CaO-$\gamma$-Al$_2$O$_3$ prepared by wet impregnation of calcium oxide precursor in $\gamma$-Al$_2$O$_3$. A commercial catalyst for methane steam reforming was also evaluated. Catalytic tests were performed at 500 °C, glycerol feed of 20% v/v and GHSV of 200,000 h$^{-1}$. The calcium oxide incorporation reduced the formation of nickel aluminate phase (NiAl$_2$O$_4$) and the amount and strength of catalyst acidity, while increasing the amount and strength of basic sites. Furthermore, it was the only catalyst that has not presented deactivation in 30 h of reaction, showing the highest glycerol conversion and hydrogen yield after 24 h of reaction. Ni/$\gamma$-Al$_2$O$_3$ and Ni/$\alpha$-Al$_2$O$_3$ presented a severe deactivation, which was associated with coke formation. The synthesized catalysts presented better catalytic performance for glycerol steam reforming in comparison with commercial catalyst, in terms of higher glycerol conversion, glycerol conversion to gas and hydrogen yield.

✉ Mariana M. V. M. Souza
mmattos@eq.ufrj.br

[1] Centro de Tecnologia, Escola de Química- Universidade Federal do Rio de Janeiro (UFRJ), Bloco E, sala 206, Rio de Janeiro, RJ CEP 21941-909, Brazil

**Graphical Abstract**
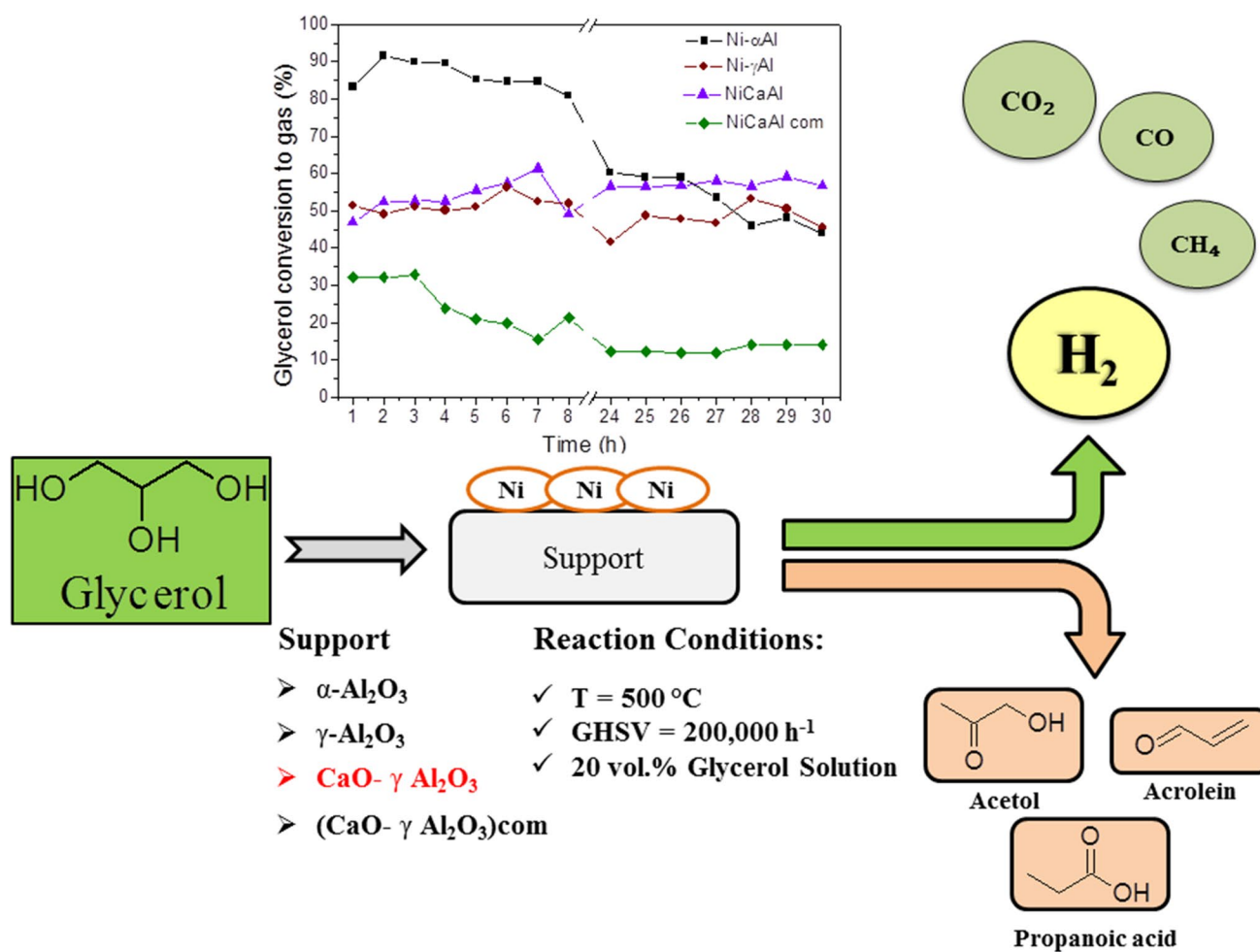


**Keywords** Glycerol · Reforming · Hydrogen · Nickel · Alumina · Calcium oxide

## 1 Introduction

Although fossil fuels played an essential role in developing many sectors of economy, these resources are non-renewable and its extensive use is related to pollutant gases emission, especially gases associated with global warming. Thus, considering the increasing concern about environmental issues, there is an urgent demand in gradually incorporate biofuels, as biodiesel and ethanol, in current energy supply matrix [1].

Biodiesel is mostly produced by oil/fat transesterification and Brazil is one of the pioneers in its production and use. Currently, ANP (Brazilian Agency for Petroleum, Natural Gas and Biofuels) stipulates the addition of 9% biodiesel in diesel, which has grown biodiesel production in the country. However, biodiesel production by transesterification generates glycerol as a byproduct, as 100 kg of glycerol is produced for each ton of biodiesel produced [2]. This produced

glycerol has lots of impurities like the catalyst, alcohols, fatty acids, salts and water, thus its direct use in usual applications, as pharmaceutical, cleaning and food industries, which require a high level of purity, is impracticable. Therefore, developing a new route for glycerol conversion into high-added value products would not only solve the problem of glycerol disposal, but would also contribute for turning biodiesel production more competitive towards diesel production. In this context, the hydrogen production by glycerol steam reforming must be highlighted.

Hydrogen is the most abundant element in the world and its use in chemical industries is indispensable. For instance, hydrogen is employed for ammonia and methanol production, for oil refining in hydrotreatment and hydrocracking processes, and for Fischer–Tropsch synthesis. Furthermore, hydrogen is considered a clean fuel, as its application in fuel cells does not release significant amount of pollutant

gases. However, most of hydrogen production currently is through natural gas (48%), heavy oils (30%) and coal (17%). Only a small part of the production is provided by water electrolysis (4%) or by biomass derivatives (1%) [3]. The study of glycerol conversion into hydrogen also intends to increase the participation of green resources in the hydrogen production matrix.

In glycerol steam reforming, synthesis gas (hydrogen and carbon monoxide) is produced by reaction of glycerol with steam, at atmospheric pressure and temperatures above 500 °C. CO is converted by shift reaction (Eq. 1) producing more hydrogen and $CO_2$. The global reforming reaction (Eq. 2) is endothermic [4].

$$CO + H_2O \leftrightarrow CO_2 + H_2 \tag{1}$$

$$C_3H_8O_3 + 3H_2O \leftrightarrow 7H_2 + 3CO_2 \tag{2}$$
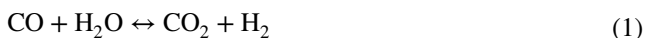
Hydrogen yield for glycerol steam reforming is higher than for methane steam reforming; for one mole of glycerol feed, seven hydrogen moles can be produced, while only three moles of hydrogen by one mole feed of methane. Furthermore, methane reforming represents a fuel consumption for producing hydrogen, which is not true for glycerol reforming [5]. Beyond that, methane reforming takes place at 700–1000 °C, while glycerol steam reforming takes place at lower temperatures.

Developing an adequate catalyst for glycerol steam reforming with good properties as high dispersion of active phase, stability, low coke and byproduct formation and high hydrogen yield, is a subject that needs investigation and further improvements. A good catalyst for glycerol reforming has to be active for the cleavage of C–C bonds and water gas shift reaction, while inhibiting the cleavage of C–O bonds and methanation reaction [6–9]. Noble metal catalysts are more active for reforming reaction and resistant to deactivation by coke deposition. However, considering the high costs of these catalysts, it is more economical the development of catalysts based on non-noble metals, as nickel or cobalt, which are also active for C–C bond cleavage [8].

γ-Alumina is the most employed support in steam reforming catalysts, because of its high surface area that leads to a good dispersion of the active phase. However, many authors have reported high coke formation on γ-alumina catalysts that causes catalyst deactivation. Silva et al. [5] suggested that coke formation occurs in γ-alumina acid sites due to dehydration, cracking and polymerization reactions. CaO has been employed as a promoter for $Ni/Al_2O_3$ catalysts used in reforming of methane, increasing conversion [10] and decreasing coke deposition [11, 12]. However, the role of CaO during glycerol steam reforming is not yet well studied; Huang et al. [13] verified that simultaneous modification of $Ni/Al_2O_3$ with Mo, La, Ca and Mg improved the catalytic stability for this reaction, while Charisiou et al. [14] recently

reported that addition of CaO–MgO to alumina not only decreased coke formation but also modified the nature of carbon deposits. Furthermore, the addition of basic promoters as Cs, Ca, Mg, Sr and Ba would enhance shift reaction, because CO adsorption and $H_2O$ dissociation are promoted by weak basic centers, and would suppress methane formation, as alkali promoters block and modify step and defect sites that are responsible for methane formation [15].

In this work, nickel catalysts with different alumina supports were evaluated in glycerol steam reforming. The novelty of the paper lies on the modification of nickel supported on alumina with calcium oxide, in order to reduce catalyst acidity and coke formation.

## 2 Experimental

### 2.1 Catalyst Preparation

Three catalysts were synthesized by wet impregnation of 20 wt% nickel precursor $[Ni(NO_3)_2 \cdot 6H_2O$ - Vetec] on different supports: $\gamma$-$Al_2O_3$ synthesized by boehmite (Sasol) calcination at 500 °C in air flow (60 mL min$^{-1}$), commercial $\alpha$-$Al_2O_3$ and 15 wt% CaO–$Al_2O_3$ synthesized by wet impregnation of calcium oxide precursor $[Ca(NO_3)_2 \cdot 4H_2O]$ on $\gamma$-$Al_2O_3$ support followed by calcination at 500 °C with air (60 mL min$^{-1}$). The catalysts were dried at 100 °C overnight and calcined at 500 °C with air (60 mL min$^{-1}$) for converting nickel nitrate into nickel oxide. The catalysts will be referred to as Ni–γAl, Ni–αAl and NiCaAl, respectively.

A commercial catalyst used for methane steam reforming was also evaluated for comparison and will be referred to as NiCaAlcom.

### 2.2 Catalyst Characterization

The chemical composition of the catalysts was verified by X-ray fluorescence (XRF) with a Rigaku Primini spectrometer.

$N_2$ adsorption–desorption experiment was carried out at − 196 °C using a Micromeritics TriStar 3000 equipment. Specific area of the catalysts was calculated by BET method and specific pore volume was determined by BJH method. The samples were outgassed and dried under vacuum for 24 h at 300 °C before the analysis.

X-ray powder diffraction (XRD) was used for determining crystalline structures of the catalysts and for nickel average crystallite size calculation before and after reaction by Scherrer equation, using the peak at 44.5º, the most intense Ni peak. The equipment used was a Rigaku Miniflex II X-ray diffractometer coupled with a graphite monochromator using CuKα radiation (30 kV and 15 mA). The analysis were conducted with a step of 0.05°, counting time of 1 s

for step and over a 2θ range of 5–90°. The reduced catalysts were analyzed after ex-situ reduction at the same conditions used in catalytic tests and spent catalysts were analyzed after reaction. Ni dispersion (D) of the catalysts was calculated according to Anderson [16] (Eq. 3).

$$D = \frac{6.Vm}{d.Am} \tag{3}$$

where Vm is the Ni atomic volume (0.0109 nm$^3$), d is the crystallite size (nm) and Am is the surface area of a single nickel atom (0.0649 nm$^2$).

Ni dispersion was also calculated by H$_2$ chemisorption, using frontal method. The analysis was conducted in an apparatus equipped with TCD for monitoring hydrogen adsorption. Prior to analysis, the catalyst (50 mg) was reduced at 800 °C with 30 mL min$^{-1}$ of H$_2$ and 60 mL min$^{-1}$ of N$_2$ flow, the same reduction condition used in catalytic test. The catalyst was heated up to 800 °C with 30mL min$^{-1}$ of a mixture 1.8% H$_2$/Ar, then a fast cooling was conducted up to 200 °C, by opening the oven, in order to detect a peak of hydrogen consumption for chemisorption on TCD signal. At 200 °C, 30mL min$^{-1}$ of argon flow was passed through the reactor for 30 min, then a fast heating rate of 120 °C min$^{-1}$ was performed up to 800 °C, in order to observe the desorption of chemisorbed hydrogen. Desorption peak was used for dispersion calculation and it was assumed that reduction degree of the catalysts prior to analysis was 100%, as they were reduced in a condition richer in hydrogen than TPR condition. Hydrogen physisorption was not considered, as temperature employed on analysis was high enough to guarantee only hydrogen chemisorption. Dispersion (D$^C$) was calculated according to Bartholomew et al. [17] (Eq. 4).

$$D^C(\%) = \frac{1.17X}{W.f} \tag{4}$$

where X is the H$_2$ uptake in μmoles per gram of the catalyst, W is the weight percentage of nickel and f is the fraction of nickel reduced to the metal, considered 100% as no nickel oxide species were observed in XRD analysis after reduction.

Temperature-programmed reduction (TPR) was used for determination of reduction profile and reducibility degree of the catalysts. The analysis was performed in a conventional apparatus equipped with a thermal conductivity detector (TCD). Prior to analysis, approximately 50 mg of the samples were treated at 150 °C under 30 mL min$^{-1}$ of argon. After the pretreatment, the reduction was conducted up to 1000 °C with a heating rate of 10 °C min$^{-1}$ under 30 mL min$^{-1}$ of a mixture 1.8% H$_2$/Ar. Reduction degree was calculated as the ratio between hydrogen consumption measured by area under TPR profile and theoretical hydrogen consumption assuming that all nickel species were reduced.

Temperature-programmed desorption of ammonia (TPD-NH$_3$) was used for catalyst acidity determination. Firstly, the reduction of the catalysts was performed at 800 °C for 30 min with a heating rate of 10 °C min$^{-1}$ and a flow rate of 30 mL min$^{-1}$ of a 1.8% H$_2$/Ar mixture. After reduction, the adsorption of ammonia was done at 70 °C for 30 min using a mixture of 4% NH$_3$/He, and the removal of physisorbed ammonia was performed with He flow of 30 mL min$^{-1}$. The ammonia desorption was conducted with a rate of 20 °C min$^{-1}$ up to 800 °C for 30 min. Ammonia consumption (ratio m/z = 15) was registered by a Pfeifer QMG-220 mass spectrometer.

Temperature-programmed desorption of CO$_2$ (TPD-CO$_2$) was performed for calculating basicity of the catalysts. Prior to analysis, 150 mg of the samples were treated at 150 °C with 30 mL min$^{-1}$ of Argon. After that, the adsorption of CO$_2$ was realized at 25 °C using a mixture 10% CO$_2$/He, and the removal of physisorbed CO$_2$ was conducted with He flow of 30 mL min$^{-1}$ for 1 h. CO$_2$ desorption was conducted with a rate of 20 °C min$^{-1}$ up to 1000 °C and the signal was registered with a TCD.

For quantifying coke deposition in spent catalysts, thermogravimetric analysis (TGA) and differential thermal analysis (DTA) with a TA SDT Q600 equipment were performed. For analysis, masses between 3 and 10 mg were weighted on the equipment itself and the analysis was carried out up to 1000 °C with a rate of 10 °C min$^{-1}$ under a synthetic air flow of 50 mL min$^{-1}$.

## 2.3 Catalytic Tests

Before the reaction beginning, 150 mg of catalysts were mixed with 750 mg of silicon carbide, which corresponds to a proportion of 1:5 (catalyst/silicon carbide). The catalysts were reduced in situ under 30% H$_2$/N$_2$ flow (90 mL min$^{-1}$) up to 800 °C at a heating rate of 10 °C min$^{-1}$ and remaining at this temperature for 30 min.

The reactions were conducted in a fixed bed quartz reactor, at 500 °C, atmospheric pressure and gas hourly space velocity (GHSV) of 200,000 h$^{-1}$. The feed consists of an aqueous solution of glycerol (20% v/v), which represents a water:glycerol molar ratio of 16.2, and was injected to the reactor by a pump (Eldex 1SAM), with flow rate of 0.106 mL min$^{-1}$. The vaporization of the solution was carried out in a vaporizer at 225 °C under He flow as a diluent; the He flow was calculated for being 20% v/v of the total gas flow (250 mL min$^{-1}$); line and valves were also kept at 225 °C for avoiding glycerol condensation.

The separation of liquid and gas phases of the product was conducted in a heat exchanger at 10 °C. The gas phase was analyzed online by a gas chromatograph (GC) Shimadzu GC-2014 equipped with two columns (RT-QPLOT and Carboxen 1010) and thermal conductivity (TCD) and

flame ionization (FID) detectors. The liquid phase was analyzed by high-performance liquid chromatography (HPLC) Shimadzu Prominence with a Bio-Rad Aminex HPX-87H column, utilizing 0.01 M $H_2SO_4$ as eluent at 0.6 mL min$^{-1}$, and with UV and refractive index detectors.

The catalyst performance was evaluated according to the equations described in Menezes et al. [18].

# 3 Results

## 3.1 Catalyst Characterization

The compositions of the calcined catalysts and of the commercial catalyst are presented in Table 1. The measured composition is similar to the desired nominal composition. The commercial catalyst also presents small amounts of magnesium and potassium oxides.

BET surface areas and pore volumes are also presented in Table 1. Ni–αAl catalyst presented the lowest BET surface area, which is in accordance with literature. Pompeo et al. [19] obtained a surface area of 10 m$^2$ g$^{-1}$ for a nickel catalyst supported on α-alumina. Ni–γAl presented the highest BET surface area and the incorporation of calcium oxide reduced BET surface area, as also observed by Dias and Assaf [10]. Adsorption–desorption isotherms of nitrogen for Ni–αAl exhibited the type II pattern, which is typical for non-porous material; on the other hand, all the other catalysts exhibited the type IV pattern, which are typical for mesoporous materials [20].

The XRD patterns of the support, calcined, reduced and spent catalysts are presented in Fig. 1. In calcined catalysts, peaks related to NiO at 2θ equal to 37.3º, 43.6º and 63.3º (JCPDS 47-1049) are observed and in reduced catalysts, peaks at 44.6º, 51.8º and 76.4º (JCPDS 04-0850) related to Ni are noticed, which proves that the reduction is efficient in converting NiO into Ni species.

A broad peak at 26°, which is related to coke deposits over catalysts throughout reaction, was observed mainly on Ni–αAl and Ni–γAl catalysts. Silicon carbide peaks were observed because its difficulty of separation from spent catalysts. Furthermore, the peaks related to nickel oxide are not observed on the spent catalysts, which indicates that reduced Ni phase is stable under reaction conditions, suggesting a good interaction between nickel phase and the supports.

Sharp peaks at 25.6º, 35.2º, 43.3º, 37.9º, 55.6º, 57.3º, 61.4º and 66.4º (JCPDS 10-173) correspond to α-alumina and are observed in all XRD profiles of Ni–αAl catalyst, presented in Fig. 1a. In Ni–γAl profiles, presented in Fig. 1b, broad peaks related to γ-alumina are observed; furthermore peaks related to spinel phase ($NiAl_2O_4$) at 37.0º, 45.0º and 65.6º (JCPDS 10-339) are also observed, and its formation is related to the strong interaction between nickel oxide and

**Table 1** Chemical composition of the catalysts, BET surface area and pore volume of the calcined catalysts, nickel crystallite size, dispersion before and after reaction calculated by Anderson correlation and dispersion before reaction calculated by $H_2$ chemisorption[c]

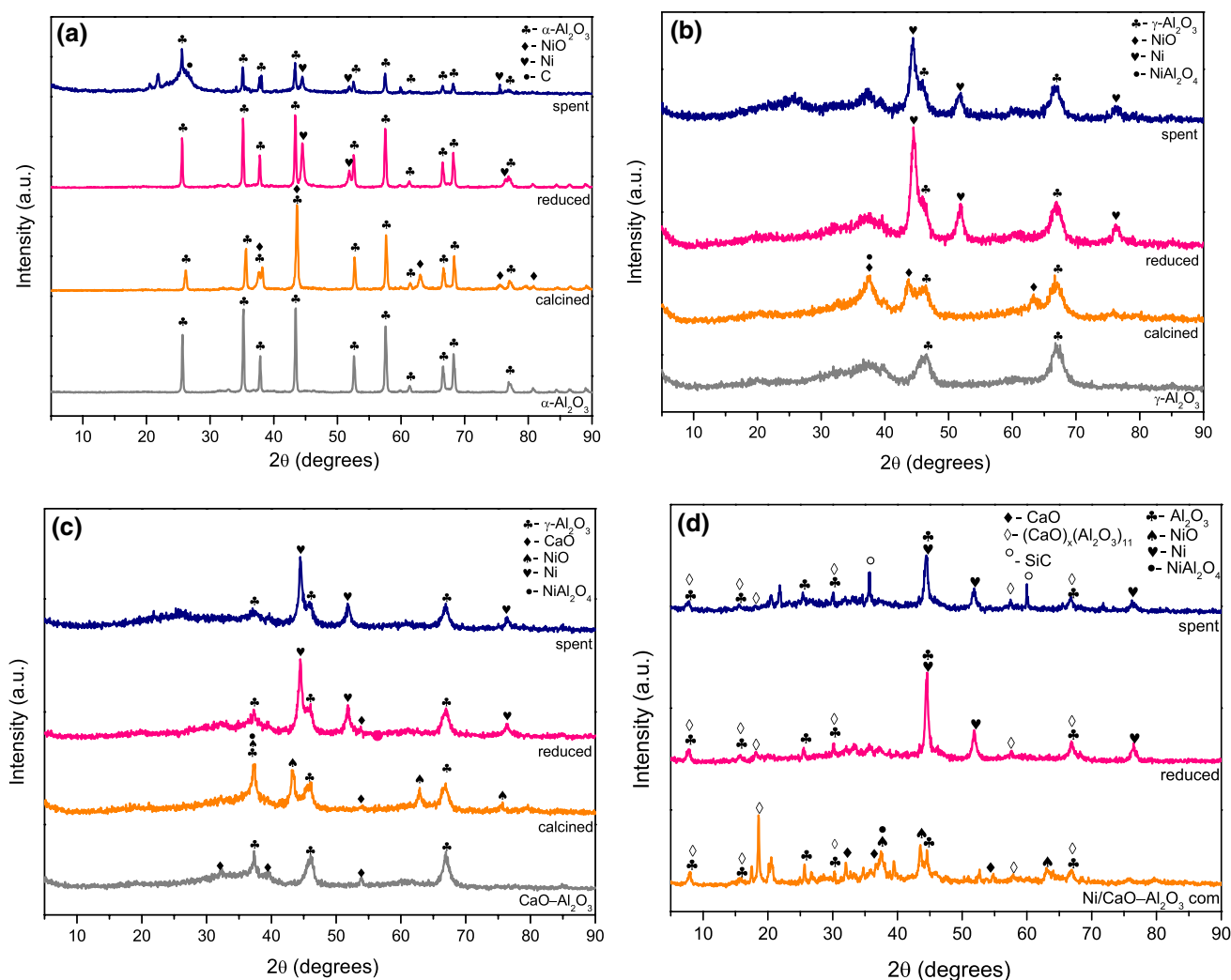| Catalyst | NiO (wt%) | CaO (wt%) | MgO (wt%) | $K_2O$ (wt%) | $S_{BET}$ (m$^2$g$^{-1}$) | $V_{Pore}$ (cm$^3$g$^{-1}$) | Ni crystallite size[a] (nm) | Ni crystallite size[b] (nm) | D[a] (%) | D[b] (%) | D[c] (%) |
|---|---|---|---|---|---|---|---|---|---|---|---|
| Ni–αAl | 26 | 0 | 0 | 0 | 12 | 0.03 | 22.9±0.8 | 23.3±3.8 | 4.4 | 4.3 | 0.6 |
| Ni–γAl | 21 | 0 | 0 | 0 | 145 | 0.34 | 8.4±2.0 | 8.4±0.7 | 12.0 | 12.0 | 1.3 |
| NiCaAl | 25 | 12 | 0 | 0 | 65 | 0.38 | 15.3±1.2 | 16.8±1.5 | 6.6 | 6.0 | 1.0 |
| NiCaAlcom | 15 | 14 | 1 | 2 | 88 | 0.13 | 18.2±1.0 | 16.2±1.1 | 5.5 | 6.2 | 1.2 |

**Fig. 1** XRD patterns of Ni–αAl **a**, Ni–γAl **b**, NiCaAl **c** and NiCaAlcom **d** catalysts

alumina. Spinel phase was not observed on NiCaAl catalyst profiles, showing that calcium oxide incorporation prevents the interaction between nickel and alumina, as observed by Wang and Lu [21] for $Ni/CeO_2/Al_2O_3$ catalysts.

Peaks related to calcium oxide at 2θ equal to 32.0, 37.4 and 53.9° (JCPDS 48-1467) are shown on XRD of NiCaAl and NiCaAlcom catalysts, presented in Fig. 1c, d respectively; however, their intensities are higher on NiCaAlcom, which indicates that calcium oxide is less dispersed on this catalyst in comparison with NiCaAl. Furthermore, peaks related to a mixed oxide $(CaO)_x(Al_2O_3)_{11}$ at 2θ equal to 7.8°, 15.8°, 30.3° and 66.8° (JCPDS 41-0358) are observed on NiCaAlcom catalyst. It is possible to observe that CaO peaks disappear after reaction, which may be related to its conversion to $Ca(OH)_2$ and/or $CaCO_3$, which may be well dispersed on alumina surface, as observed by other authors [22, 23].

The mean nickel crystallite sizes were determined before and after reaction using nickel peak at 44.5° on

XRD profiles of the reduced and spent catalysts and are shown in Table 1, which also shows the nickel dispersion determined by Anderson correlation. Ni–αAl presented the biggest nickel crystallite size (22.9 nm) and the lowest dispersion (4.4%) among the catalysts, which is in accordance with its lowest BET surface area (Table 1). Moreover, the addition of calcium oxide on alumina support increased the nickel crystallite size and decreased noticeably the dispersion in comparison with the catalyst without calcium oxide. This result agrees with the decreasing on BET surface area from 145 to 65 $m^2\ g^{-1}$ with calcium oxide incorporation, which may cover and block alumina pores. Nickel dispersion is higher for NiCaAl than for NiCaAlcom.

Considering the analysis error, it was not possible to observe significant difference between nickel crystallite sizes before and after reaction, which suggests that sintering process is not significant for these catalysts. NiCaAl catalyst

presented the highest increase in crystallite size, from 15.3 to 16.8 nm, which is irrelevant.

Ni dispersion was also measured by hydrogen chemisorption and the results are presented in Table 1. Comparing with the results obtained from XRD, it is possible to observe that the values are much lower, which it is expected as XRD is a bulk technique and $H_2$ chemisorption quantifies only surface nickel species. However, both results followed the same tendency, as Ni–αAl has presented the lowest dispersion (0.6%) and Ni–γAl has presented the highest dispersion (1.3%). These results are in accordance with other authors in the literature. Cheng et al. [24] obtained a dispersion of 0.74% for 5 wt% Co–10 wt% $Ni/Al_2O_3$ by hydrogen chemisorption and this low metal dispersion was attributed to the high metal loading (15 wt%) employed. Jing et al. [25] reported values of 0.84–1.07% for Ni dispersion on 15%Ni/ $CaO–Al_2O_3$ catalysts prepared by coprecipitation, with different Ca/Al ratios.

Figure 2 shows the TPR analysis of the catalysts. Ni–γAl and Ni–αAl catalysts presented only one reduction peak centered at 800 °C and 440 °C, respectively. Rynkowski et al. [26] reported the existence of three different nickel species in a catalyst supported on alumina: bulk NiO, with reduction peak below 400 °C, NiO interacting with alumina, with

reduction peaks between 400 and 690 °C, and NiO incorporated on alumina for aluminate spinel phase formation, with reduction peak above 700 °C. Thus, it is possible to infer the existence of $NiAl_2O_4$ species on Ni–γAl catalyst, which is in agreement with XRD analysis.

Reduction profile of NiCaAl presented one peak at 335 °C, related to bulk NiO, four peaks between 400 and 800 °C, which are associated with NiO interacting with $Al_2O_3$ and CaO in different levels of interaction, and one peak located at 895 °C, related to nickel aluminate reduction. Comparing NiCaAl and Ni–γAl TPR profiles, it is possible to observe a decrease of nickel aluminate formation, because the peak located above 700 °C has a higher area for Ni–γAl catalyst. This result corroborates the decrease of nickel dispersion by calcium oxide incorporation, caused by reduction of interaction between nickel species and the support. The formation of nickel species with low interaction with alumina when calcium is added to the support was also observed by Dias and Assaf [10] and Ashok et al. [22].

Reduction profile of NiCaAlcom catalyst presented three overlapping peaks in the range of 500–950 °C, the first located at 600 °C, the second at 678 °C and the last at 788 °C. There is also a small peak located at 386 °C, however the major reduction of NiO species occurs in temperatures above 400 °C, which indicates a stronger interaction between nickel oxide and the support for NiCaAlcom catalyst.

The reduction degrees of the catalysts are shown in Table 2. The lowest reduction degree (54%) was observed for Ni–αAl catalyst, which is associated with its biggest Ni crystallite size, because inner nickel oxide particles are more inaccessible for hydrogen molecules, so the reduction is limited.

TPD-$NH_3$ profiles of the catalysts are shown in Fig. 3 and calculated acidity is presented in Table 2. The literature classifies peaks below 400 °C as weak acid sites, while above this temperature the sites are classified as strong acid sites [27]. Thus, all the catalysts have presented mainly weak acid sites. Ni–αAl catalyst showed no $NH_3$ desorption peaks, therefore its acidity is zero, which was expected because of its low BET area. Ni–γAl and NiCaAl presented similar profiles, with peaks centered at 186 °C and 163 °C, respectively. However, the acidity per area is higher for Ni–γAl
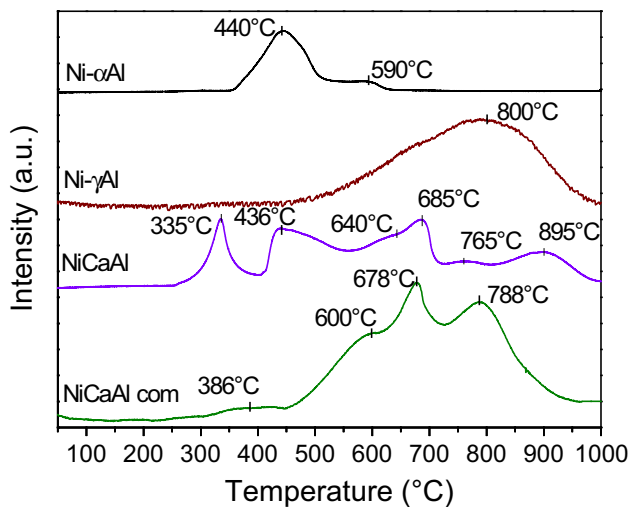


**Fig. 2** TPR profiles of the calcined catalysts

**Table 2** Hydrogen uptake and reduction degree (RD) of NiO calculated from TPR results, amount of desorbed $NH_3$ per mass and per BET area calculated from TPD-$NH_3$ results and amount of desorbed $CO_2$ from TPD-$CO_2$

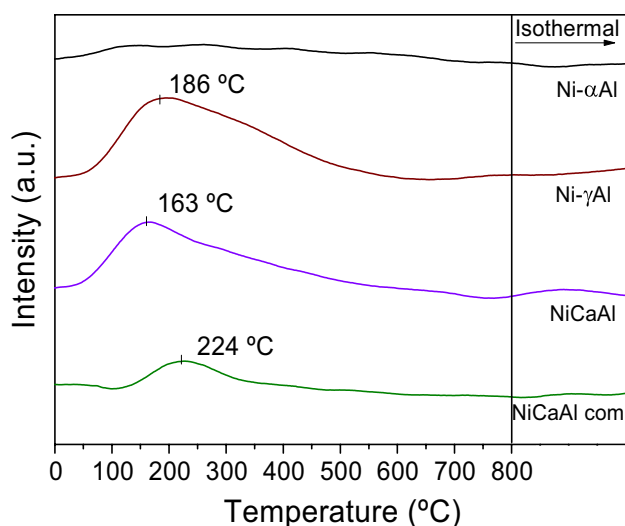| Catalyst | µmol $H_2$ gcat$^{-1}$ | RD (%) | µmol $NH_3$ gcat$^{-1}$ | µmol $NH_3$ m$^{-2}$ | µmol $CO_2$ m$^{-2}$ |
|---|---|---|---|---|---|
| Ni–αAl | 1964.8 | 54 | 0.0 | 0.0 | 2.7 |
| Ni–γAl | 2526.0 | 90 | 458.9 | 3.1 | 6.2 |
| NiCaAl | 3243.5 | 97 | 105.4 | 1.6 | 14.9 |
| NiCaAlcom | 1993.1 | 100 | 24.1 | 0.3 | 3.3 |

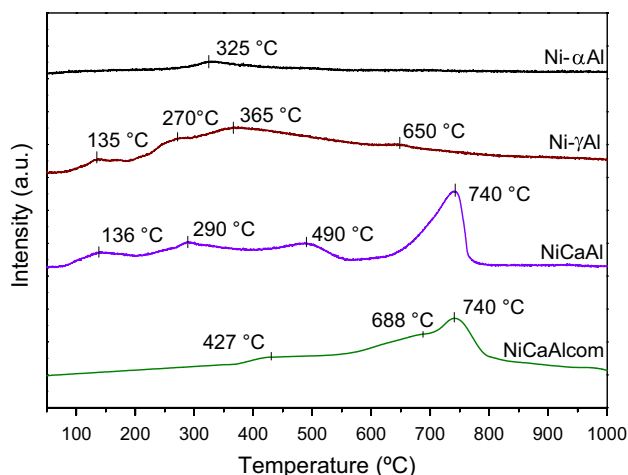**Fig. 3** TPD-NH$_3$ profiles of the reduced catalysts



**Fig. 4** TPD-CO$_2$ profiles of the catalysts

catalyst, as also the strength of acid sites, because of the higher temperature of desorption. Thus, the addition of a basic promoter, as calcium oxide, reduced the acidity, which was also observed by Sánchez-Sánchez et al. [28]. NiCaAl-com catalyst presented lower acidity than NiCaAl, which can be explained by the presence of small amounts of other promoters, as MgO and K$_2$O, or by the different synthesis method.

TPD-CO$_2$ profiles of the catalysts are presented in Fig. 4 and the values of basicity normalized by BET surface area are shown in Table 2. First, it is observed that calcium oxide addition shifted CO$_2$ desorption peaks for higher temperatures, indicating stronger basic sites. Ni–γAl presented three broad desorption peaks in the region of 100–500 °C and only a small peak at 650 °C, while NiCaAl catalyst presented the

most intense CO$_2$ desorption peak at 740 °C. Ashok et al. [29] also observed two regions of CO$_2$ desorption for Ni–Fe catalysts supported on calcium oxide and alumina. The first region from 100 to 350 °C was assigned to low-strength basic sites, such as bicarbonates that result from the interactions between CO$_2$ and weak basic surface hydroxyl groups, while the second region from 400 to 600 °C was associated with high-strength basic sites, such as unidentate carbonates, formed in the presence of over-saturated CaO species. In this work, the peak observed at high temperature (740 °C) on both NiCaAl and NiCaAlcom catalysts were more intense than peaks observed at low temperatures, indicating the presence of high amount of over-saturated CaO species. Ni–αAl catalyst presented only a small peak located at 325 °C, which was expected because of its low BET surface area.

The results of basicity presented in Table 2 show an increase in the amount of basic sites by CaO incorporation, as NiCaAl presented the highest basicity (14.9 μmol CO$_2$ m$^{-2}$) and Ni–γAl presented basicity of 6.2 μmol CO$_2$ m$^{-2}$. These results of basicity are in agreement with the values obtained by Ashok et al. [29] for Ni–Fe catalysts supported on alumina promoted with various amounts of calcium oxide (0.5–2 wt%); they found basicity values from 16.4 μmol CO$_2$ m$^{-2}$ for the catalyst promoted with 0.5 wt% of CaO to 24.7 μmol CO$_2$ m$^{-2}$ for the catalyst promoted with 2 wt%.

## 3.2 Catalytic Tests

Glycerol conversion and glycerol conversion to gas are presented in Fig. 5a, b, respectively. Ni–αAl and Ni–γAl obtained the highest glycerol conversion in the first 8 h of reaction, with glycerol conversion in the range of 85–100%. However, they suffered a severe deactivation after 24 h of reaction. Ni–γAl conversion decayed to 67% in 24 h of reaction and was kept constant between 67 and 77%; on the other hand, Ni–αAl conversion was reduced to 61% and was kept constant between 61 and 67%. Thus, the deactivation of Ni–αAl catalyst was more severe, which can be explained by the lowest reduction degree, lowest nickel dispersion and highest coke formation, as will be seen later. The deactivation of nickel catalysts supported on alumina has been widely reported in the literature. Sánchez et al. [30] observed deactivation of Ni catalysts supported on γ-alumina after 8 h of reaction at 600 °C and 650 °C.

NiCaAlcom presented the lowest glycerol conversion and glycerol conversion to gas during all reaction time and also presented deactivation as glycerol conversion was reduced from 68% in the first hour to 40% in 24 h of reaction. This worst catalytic performance may be explained by the lower Ni dispersion in comparison with NiCaAl and Ni–γAl; furthermore, it presented lower nickel content, thus the availability of nickel species is lower for this catalyst. In contrast, NiCaAl catalyst was the only catalyst without
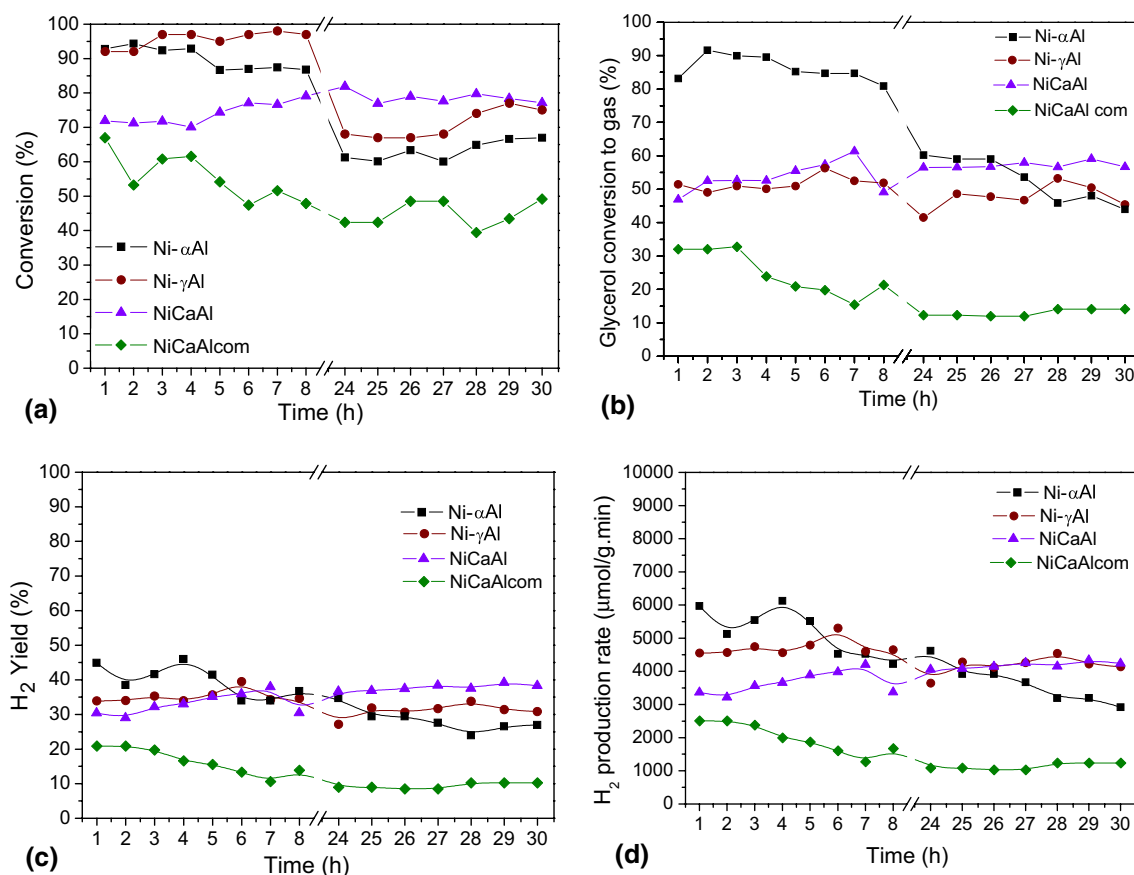
**Fig. 5** Glycerol conversion (**a**), glycerol conversion into gas (**b**), H$_2$ yield (**c**), and hydrogen production rate (**d**) for the catalysts during glycerol steam reforming. Reaction conditions: 500 °C, GHSV of 200,000 h$^{-1}$ and 20% v/v glycerol solution

any deactivation during reaction time: glycerol conversion was kept between 70 and 80% during all reaction time and was higher than glycerol conversion of Ni–γAl after 24 h of reaction.

The difference between glycerol conversion and glycerol conversion to gas for all the catalysts, except for Ni–αAl, may be explained by liquid byproduct formation (acrolein, acetol and propanoic acid). Ni–αAl was the only catalyst in which the glycerol conversion and glycerol conversion to gas are almost the same during reaction time, which indicates low byproduct formation. Ni–γAl presented the highest difference in the first hour of reaction, as glycerol conversion was 98% and glycerol conversion to gas was around 50%; this behavior suggests not only liquid byproduct formation but also high coke formation in the first hour of reaction, which explains the fast deactivation. NiCaAl and NiCaAl-com presented similar behavior of glycerol conversion and glycerol conversion to gas, with a difference around 20% between both parameters, suggesting that coke formation was better distributed in reaction time, so deactivation was less severe for these catalysts in comparison with Ni–γAl catalyst.

Figure 5c, d shows hydrogen yield and hydrogen production rate during reaction time. It is possible to observe that Ni–αAl, Ni–γAl and NiCaAl showed a similar behavior, with mean H$_2$ yields of 37, 33 and 35%, respectively. Hydrogen mean production rate was 4900, 4400 and 3900 μmol H$_2$g$^{-1}$ min$^{-1}$, respectively. On the other hand, NiCaAlcom presented the lowest mean hydrogen yield (13%) and lowest hydrogen production rate, around 1600 μmol H$_2$g$^{-1}$ min$^{-1}$. This result is associated with the lowest glycerol conversion to gas and indicates a low activity for glycerol reforming and shift reactions.

Figure 6 shows selectivities for reforming gases: H$_2$, CO, CO$_2$ and CH$_4$. It is observed that Ni–αAl presented the lowest hydrogen selectivity which suggests that hydrogen generated in reforming is being consumed for coke formation by CO and CO$_2$ hydrogenation (Eq. 5 and 6), or by methane formation by methanation reactions (Eq. 7 and 8).
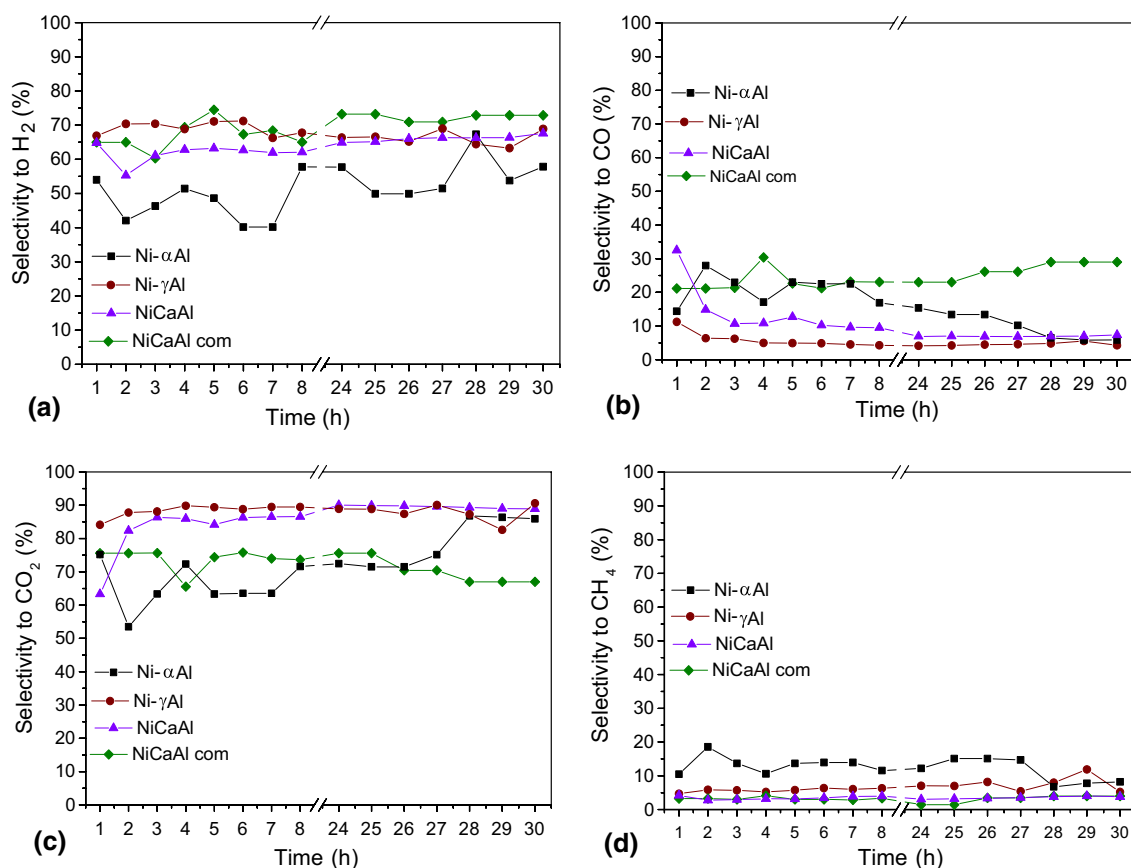
$$CO + H_2 \leftrightarrow C + H_2O \tag{5}$$

$$CO_2 + 2H_2 \leftrightarrow 2H_2O + C \tag{6}$$

$$CO + 3H_2 \leftrightarrow CH_4 + H_2O \tag{7}$$

**Fig. 6** Selectivities to $H_2$ (**a**), CO (**b**), $CO_2$ (**c**) and $CH_4$ (**d**) for the catalysts. Reaction conditions: 500 °C, GHSV of 200,000 $h^{-1}$ and 20% v/v glycerol solution

$$CO_2 + 4H_2 \leftrightarrow CH_4 + 2H_2O \tag{8}$$

Analyzing the first 8 h of reaction, Ni–αAl presented superior selectivity to CO and lower selectivity to $CO_2$ than NiCaAl and Ni–γAl, which suggests a low activity for shift reaction for Ni–αAl catalyst. Moreover, it was noticed that $CO_2$ selectivity increases and CO selectivity decreases throughout reaction time, which suggests that CO is being consumed for coke formation by CO disproportionation reaction as presented in Eq. 9.

$$2CO \leftrightarrow CO_2 + C \tag{9}$$

A high activity for shift reaction was observed for NiCaAl and Ni–γAl catalysts, expressed by the lowest CO and highest $CO_2$ selectivities, which enhances hydrogen production. NiCaAlcom is not very active for shift reaction, as can be observed by high CO and low $CO_2$ selectivities. NiCaAlcom presented the highest CO mean selectivity (25%). For this catalyst, CO selectivity decreases from 32% in the first hour to 7% after 24 h of reaction.

Ni–αAl catalyst showed the highest mean methane selectivity (12%). This high selectivity in comparison with the other catalysts is associated with the highest activity to methanation reactions, as already mentioned before, corroborating the lowest hydrogen selectivity for this catalyst.

Table 3 shows liquid byproducts yields: acrolein, acetol and propanoic acid. Acrolein and acetol are produced by glycerol dehydration (Eqs. 10 and 11), and acrolein formation takes place mainly in Bronsted acid sites of the support, as it was observed by several authors [31–33]. Propanoic acid is produced by acetol isomerization (Eq. 12) as observed by Corma et al. [34].
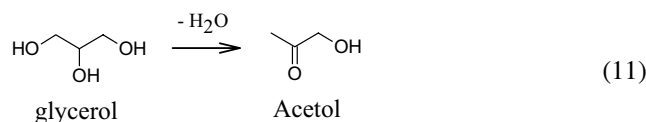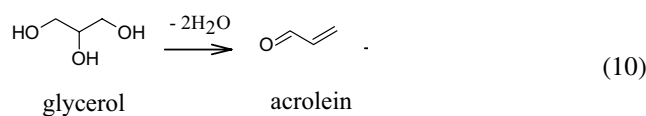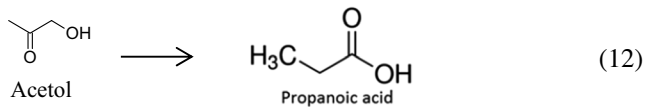


$$\tag{10}$$



$$\tag{11}$$

**Table 3** Acrolein ($Y_{acr}$), acetol ($Y_{ace}$) and propanoic acid ($Y_{acp}$) average yields and coke formation measured by TGA analysis

| Catalyst | $Y_{acr\ (1-8\ h)}$ | $Y_{acr\ (24-30\ h)}$ | $Y_{ace\ (1-8\ h)}$ | $Y_{ace\ (24-30\ h)}$ | $Y_{acp\ (1-8\ h)}$ | $Y_{acp\ (24-30\ h)}$ | Coke (%) |
|---|---|---|---|---|---|---|---|
| Ni–αAl | 0.1 | 0.1 | 2.2 | 2.6 | 0.4 | 0.6 | 59.1 |
| Ni–γAl | 7.6 | 1.0 | 6.7 | 2.3 | 2.7 | 0.7 | 31.9 |
| NiCaAl | 5.9 | 6.0 | 28.4 | 26.2 | 11.6 | 8.8 | 32.9 |
| NiCaAlcom | 3.5 | 3.6 | 12.4 | 13.2 | 4.3 | 3.9 | 22.5 |

$$\text{Acetol} \longrightarrow \text{Propanoic acid} \qquad (12)$$

Ni–αAl catalyst showed the lowest byproduct yields, which corroborates the low difference between glycerol conversion and conversion to gas. This may be explained by its low surface area and no availability of support acid sites for byproduct formation. The mean byproduct yields for this catalyst were 0.1% for acrolein, 2.4% for acetol and 0.5% for propanoic acid. On the other hand, Ni–γAl catalyst presented the highest acrolein yield in the first 8 h of reaction, which is associated with its highest acidity. The mean acrolein yield in the first 8 h was 8.6% and decreased for 1% in the last 7 h

of reaction, which is associated with coke formation that may cover alumina acid sites.

The catalysts with basic promoters, NiCaAl and NiCa-Alcom, presented the highest acetol and propanoic acid yields during all reaction time. Mean propanoic acid yields were 10.3% for NiCaAl and 4.1% for NiCaAlcom; and mean acetol yields were 27.4% for NiCaAl and 12.8% for NiCa-Alcom. Stošić et al. [35] studied the effect of acid-basic catalytic properties on glycerol dehydration and reported that, differently from acrolein formation that is favored on Bronsted acid sites, acetol yield increases with reduction in amount and strength of acid sites.

TGA and DTA analysis are presented in Fig. 7 and the amount of coke is shown in Table 3. The deactivation noticed for the catalysts are related with coke formation. The highest coke formation (59.1%) was observed for Ni–αAl catalyst, which corroborates its severe deactivation. A big
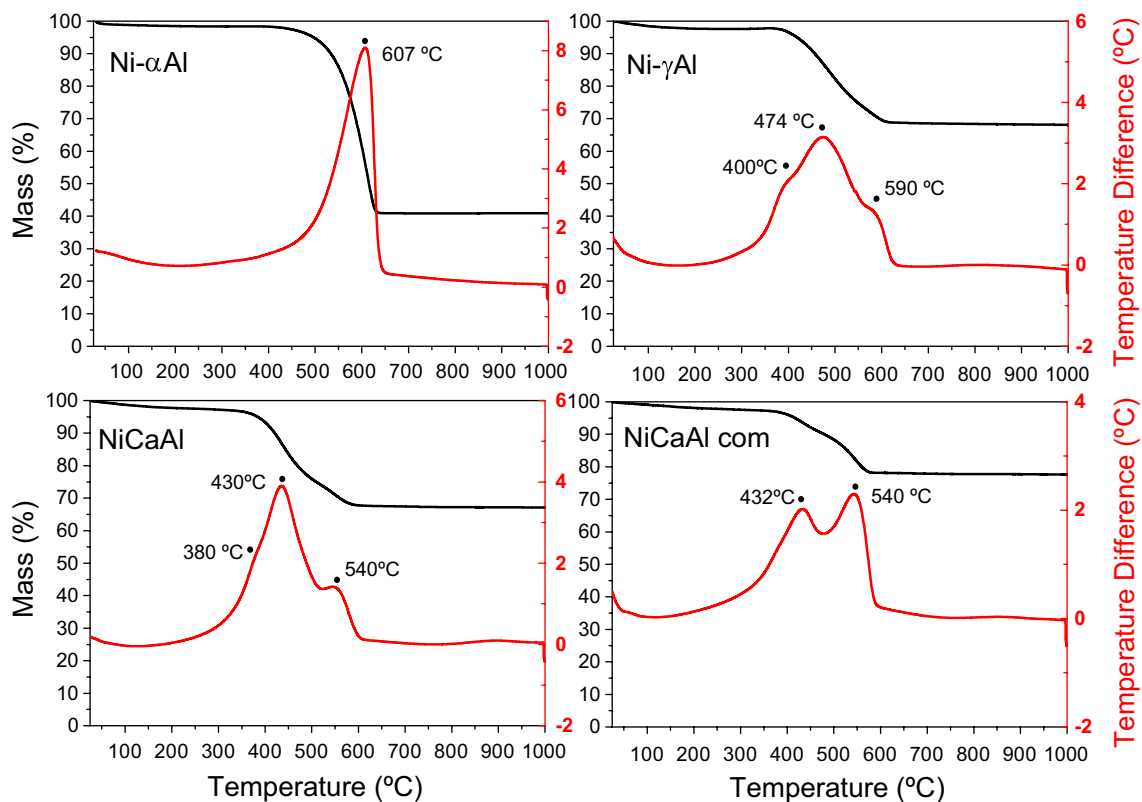


**Fig. 7** TGA and DTA of the spent catalysts

nickel crystallite size, observed for Ni–αAl catalyst, may have contributed for its deactivation, because coke is formed preferentially in the presence of big crystallite sizes, as reported by Lisboa et al. [36].

Acid sites presented on Ni–γAl, NiCaAl and NiCaAlcom catalysts may be associated with coke formation, as reported by Atia et al. [31]. According to the literature, amorphous coke presents a lower oxidation temperature in comparison with filamentous coke [37]. Thus, it is observed that Ni–αAl presented higher amount of filamentous coke and the catalysts modified with calcium oxide, NiCaAl and NiCaAlcom, presented higher amount of amorphous coke, as calcium oxide addition in NiCaAl catalyst shifted DTA peaks for lower temperatures; the main DTA peak for Ni–γAl is located at 474 °C and for NiCaAl is located at 430 °C. The tendency of CaO–MgO modified catalyst to form lower amount of coke, and with lower oxidation temperature, as compared to Ni/Al$_2$O$_3$, was also observed by Charisiou et al. [14]. Ashok et al. [37] attributed the lower oxidation temperature of coke formed on Ni/CaO–Al$_2$O$_3$–CeO$_2$ to the superior and stable catalytic performance of this catalyst in comparison with the catalyst with no ceria doping for toluene steam reforming, relating the lower temperature of oxidation with a more easily gasification of surface carbon. This is in agreement with our results, as NiCaAl catalyst presented a coke with lower oxidation temperature than Ni–γAl catalyst, which contributed for its higher stability during reaction time.

## 4 Conclusions

Three nickel catalysts, supported on alpha alumina (Ni–αAl), gamma alumina (Ni–γAl) and CaO/γ-Al$_2$O$_3$ (NiCaAl) were synthesized by wet impregnation of nickel precursors on supports and evaluated in glycerol steam reforming at 500 °C, during 30 h. A fourth commercial catalyst for methane steam reforming (NiCaAlcom) was also evaluated in glycerol steam reforming. NiCaAl catalyst was the only catalyst that did not present any deactivation during all reaction time, with glycerol conversion to gas of approximately 55% and hydrogen yield of approximately 35%. The incorporation of calcium oxide reduced nickel dispersion and BET surface area, besides decreasing the catalyst acidity and acid strength, which are related to coke formation. Moreover, nickel aluminate formation was reduced by CaO addition, decreasing the reduction temperature. The incorporation of calcium oxide also favored the formation of a more easily removable carbon, which explained the deactivation for Ni–γAl and non-deactivation for NiCaAl.

Ni–αAl catalyst presented the lowest BET surface area, nickel dispersion and its acidity was zero. This catalyst suffered severe deactivation mainly by coke formation, as shown by TG analysis. The consumption of hydrogen for coke and methane formation explained the lowest hydrogen selectivity for this catalyst. NiCaAlcom catalyst presented the worst catalytic performance in terms of glycerol conversion, conversion to gas and hydrogen production, with low activity for shift reaction.

In terms of liquid byproduct formation, calcium oxide addition reduced acrolein formation but increased acetol and propanoic formation in comparison with Ni–γAl catalyst. On the other hand, Ni–αAl catalyst presented insignificant liquid byproduct formation, explained by its lowest BET area and acidity.

## References

1. Shahid EM, Jamal Y (2008) A review of biodiesel as vehicular fuel. Renew Sustain Energy Rev 12:2477–2487. https://doi.org/10.1016/j.rser.2007.06.001
2. Adhikari S, Fernando SD, Filip To SD et al (2008) Conversion of glycerol to hydrogen via a steam reforming process over nickel catalysts. Energy Fuels 22:1220–1226. https://doi.org/10.1021/ef700520f
3. Balat H, Kirtay E (2010) Hydrogen from biomass - Present scenario and future prospects. Int J Hydrog Energy 35:7416–7426. https://doi.org/10.1016/j.ijhydene.2010.04.137
4. Wang C, Dou B, Chen H et al (2013) Hydrogen production from steam reforming of glycerol by Ni–Mg–Al based catalysts in a fixed-bed reactor. Chem Eng J 220:133–142. https://doi.org/10.1016/j.cej.2013.01.050
5. Silva JM, Soria MA, Madeira LM (2015) Challenges and strategies for optimization of glycerol steam reforming process. Renew Sustain Energy Rev 42:1187–1213. https://doi.org/10.1016/j.rser.2014.10.084
6. Davda RR, Shabaker JW, Huber GW et al (2005) A review of catalytic issues and process conditions for renewable hydrogen and alkanes by aqueous-phase reforming of oxygenated hydrocarbons over supported metal catalysts. Appl Catal B 56:171–186. https://doi.org/10.1016/j.apcatb.2004.04.027
7. Cortright RD, Davda RR, Dumesic JA (2002) Hydrogen from catalytic reforming of biomass-derived hydrocarbons in liquid water. Nature 418:964–967. https://doi.org/10.1038/nature01009
8. Shabaker JW, Davda RR, Huber GW et al (2003) Aqueous-phase reforming of methanol and ethylene glycol over alumina-supported platinum catalysts. J Catal 215:344–352. https://doi.org/10.1016/S0021-9517(03)00032-0
9. Shabaker JW, Huber GW, Dumesic JA (2004) Aqueous-phase reforming of oxygenated hydrocarbons over Sn-modified Ni catalysts. J Catal 222:180–191. https://doi.org/10.1016/j.jcat.2003.10.022
10. Dias JAC, Assaf JM (2003) Influence of calcium content in Ni/CaO/γ-Al$_2$O$_3$ catalysts for CO$_2$-reforming of methane. Catal Today 85:59–68. https://doi.org/10.1016/S0920-5861(03)00194-9
11. Quinconces CE, Dicundo S, Alvarez AM, González MG (2001) Effect of addition of Cao on Ni/Al$_2$O$_3$ catalysts over CO$_2$ reforming of methane. Mater Lett 50:21–27. https://doi.org/10.1007/s10562-011-0685-0

12. Alipour Z, Rezaei M, Meshkani F (2014) Effect of alkaline earth promoters (MgO, CaO, and BaO) on the activity and coke formation of Ni catalysts supported on nanocrystalline $Al_2O_3$ in dry reforming of methane. J Ind Eng Chem 20:2858–2863. https://doi.org/10.1016/j.jiec.2013.11.018

13. Huang ZY, Xu CH, Liu CQ et al (2013) Glycerol steam reforming over Ni/γ-$Al_2O_3$ catalysts modified by metal oxides. Korean J Chem Eng 30:587–592. https://doi.org/10.1007/s11814-012-0204-z

14. Charisiou ND, Papageridis KN, Tzounis L et al (2018) Ni supported on CaO–MgO–$Al_2O_3$ as a highly selective and stable catalyst for H2 production via the glycerol steam reforming reaction. Int J Hydrog Energy. https://doi.org/10.1016/j.ijhydene.2018.02.165

15. Ashok J, Wai MH, Kawi S (2018) Nickel-based catalysts for high-temperature water gas shift reaction-methane suppression. Chem Cat Chem 10:3927–3942. https://doi.org/10.1002/cctc.201800031

16. Anderson JR (1975) Structure of metallic catalysts. Academic Press, London

17. Bartholomew CH, Pannell RB (1980) The stoichiometry of hydrogen and carbon monoxide chemisorption on alumina- and silica-supported nickel. J Catal 65:390–401. https://doi.org/10.1016/0021-9517(80)90316-4

18. da Menezes JPSQ, Manfro RL, Souza MMVM (2018) Hydrogen production from glycerol steam reforming over nickel catalysts supported on alumina and niobia: deactivation process, effect of reaction conditions and kinetic modeling. Int J Hydrog Energy 43:15064–15082. https://doi.org/10.1016/j.ijhydene.2018.06.048

19. Pompeo F, Nichio NN, Ferretti OA, Resasco D (2005) Study of Ni catalysts on different supports to obtain synthesis gas. Int J Hydrog Energy 30:1399–1405. https://doi.org/10.1016/j.ijhydene.2004.10.004

20. Sing KSW (1985) Reporting physisorption data for gas/solid systems with special reference to the determination of surface area and porosity. Pure Appl Chem 57:603–619. https://doi.org/10.1351/pac198557040603

21. Wang S, Lu GQM (1998) Role of $CeO_2$ in Ni/$CeO_2$–$Al_2O_3$ catalysts for carbon dioxide reforming of methane. Appl Catal B 19:7435–7443. https://doi.org/10.1016/S1004-9541(14)60029-X

22. Ashok J, Kathiraser Y, Ang ML, Kawi S (2015) Bi-functional hydrotalcite-derived NiO–CaO–$Al_2O_3$ catalysts for steam reforming of biomass and/or tar model compound at low steam-to-carbon conditions. Appl Catal B 172–173:116–128. https://doi.org/10.1016/j.apcatb.2015.02.017

23. Hildenbrand N, Readman J, Dahl IM, Blom R (2006) Sorbent enhanced steam reforming (SESR) of methane using dolomite as internal carbon dioxide absorbent: limitations due to Ca(OH)$_2$ formation. Appl Catal A 303:131–137. https://doi.org/10.1016/j.apcata.2006.02.015

24. Cheng CK, Foo SY, Adesina AA (2010) Glycerol steam reforming over bimetallic Co–Ni/$Al_2O_3$. Ind Eng Chem Res 49:10804–10817. https://doi.org/10.1021/ie100462t

25. Jing J, Wang S, Zhang X et al (2017) Influence of Ca/Al molar ratio on structure and catalytic reforming performance of Ni/CaO–$Al_2O_3$ catalyst. J Fuel Chem Technol 45:956–962. https://doi.org/10.1016/s1872-5813(17)30046-4

26. Rynkowski JM, Paryjczak T, Lenik M (1993) On the nature of oxidic nickel phases in NiO/γ-$Al_2O_3$ catalysts. Appl Catal A 106:73–82. https://doi.org/10.1016/0926-860X(93)80156-K

27. Ribeiro NFP, Henriques CA, Schmal M (2005) Copper-based catalysts for synthesis of methylamines: the effect of the metal and the role of the support. Catal Lett 104:111–119. https://doi.org/10.1007/s10562-005-7939-7

28. Sánchez-Sánchez MC, Navarro RM, Fierro JLG (2007) Ethanol steam reforming over Ni/MxOy–$Al_2O_3$(M = Ce, La, Zr and Mg) catalysts: influence of support on the hydrogen production. Int J Hydrog Energy 32:1462–1471. https://doi.org/10.1016/j.ijhydene.2006.10.025

29. Ashok J, Kawi S (2015) Steam reforming of biomass tar model compound at relatively low steam-to-carbon condition over CaO-doped nickel-iron alloy supported over iron-alumina catalysts. Appl Catal A 490:24–35. https://doi.org/10.1016/j.apcata.2014.10.057

30. Sánchez EA, D'Angelo MA, Comelli RA (2010) Hydrogen production from glycerol on Ni/$Al_2O_3$ catalyst. Int J Hydrog Energy 35:5902–5907. https://doi.org/10.1016/j.ijhydene.2009.12.115

31. Atia H, Armbruster U, Martin A (2011) Influence of alkaline metal on performance of supported silicotungstic acid catalysts in glycerol dehydration towards acrolein. Appl Catal A 393:331–339. https://doi.org/10.1016/j.apcata.2010.12.015

32. Haider MH, Dummer NF, Zhang D et al (2012) Rubidium- and caesium-doped silicotungstic acid catalysts supported on alumina for the catalytic dehydration of glycerol to acrolein. J Catal 286:206–213. https://doi.org/10.1016/j.jcat.2011.11.004

33. Manfro RL, Pires TPMD, Ribeiro NFP, Souza MMVM (2013) Aqueous-phase reforming of glycerol using Ni–Cu catalysts prepared from hydrotalcite-like precursors. Catal Sci Technol 3:1278–1287. https://doi.org/10.1039/c3cy20770f

34. Corma A, Huber GW, Sauvanaud L, O'Connor P (2008) Biomass to chemicals: catalytic conversion of glycerol/water mixtures into acrolein, reaction network. J Catal 257:163–171. https://doi.org/10.1016/j.jcat.2008.04.016

35. Stošić D, Bennici S, Sirotin S et al (2012) Glycerol dehydration over calcium phosphate catalysts: effect of acidic-basic features on catalytic performance. Appl Catal A 447–448:124–134. https://doi.org/10.1016/j.apcata.2012.09.029

36. Lisboa JDS, Santos DCRM, Passos FB, Noronha FB (2005) Influence of the addition of promoters to steam reforming catalysts. Catal Today 101:15–21. https://doi.org/10.1016/j.cattod.2004.12.005

37. Ashok J, Kawi S (2013) Steam reforming of toluene as a biomass tar model compound over $CeO_2$ promoted Ni/CaO–$Al_2O_3$ catalytic systems. Int J Hydrog Energy 38:13938–13949. https://doi.org/10.1016/j.ijhydene.2013.08.029